Laminated Carbon Nanotube Networks for Metal Electrode-Free Efficient Perovskite Solar Cells

Zhen Li,[†] Sneha A. Kulkarni,[†] Pablo P. Boix,[†] Enzheng Shi,[§] Anyuan Cao,[§] Kunwu Fu,[†,‡] Sudip K. Batabyal,[†] Jun Zhang,[⊥] Qihua Xiong,[⊥] Lydia Helena Wong,[†,‡,*] Nripan Mathews,[†,‡,∥,*] and Subodh G. Mhaisalkar[†,‡]

[†]Energy Research Institute at NTU (ERI@N), Nanyang Technological University, Techno Plaza, 50 Nanyang Drive, 637553, Singapore, [‡]School of Materials Science and Engineering, Nanyang Technological University (NTU), Block N4.1, Nanyang Avenue, 639798, Singapore, [∥]Singapore-Berkeley Research Initiative for Sustainable Energy, 1 Create Way, 138602, Singapore, [§]Department of Materials Science and Engineering, College of Engineering, Peking University, Beijing, 100871, People's Republic of China, and [⊥]Division of Physics and Applied Physics, School of Physical and Mathematical Sciences, Nanyang Technological University, 637371, Singapore

ABSTRACT Organic—inorganic metal halide perovskite solar cells were fabricated by laminating films of a carbon nanotube (CNT) network onto a $CH_3NH_3PbI_3$ substrate as a hole collector, bypassing the energy-consuming vacuum process of metal deposition. In the absence of an organic hole-transporting material and metal contact, $CH_3NH_3PbI_3$ and CNTs formed a solar cell with an efficiency of up to 6.87%. The $CH_3NH_3PbI_3$/CNTs solar cells were semitransparent and showed photovoltaic output with dual side illuminations due to the transparency of the CNT electrode. Adding spiro-OMeTAD to the CNT network forms a composite electrode that improved the efficiency to 9.90% due to the enhanced hole extraction and reduced recombination in solar cells. The interfacial charge transfer and transport in solar cells were investigated through photoluminescence and impedance measurements. The flexible and transparent CNT network film shows great potential for realizing flexible and semitransparent perovskite solar cells.

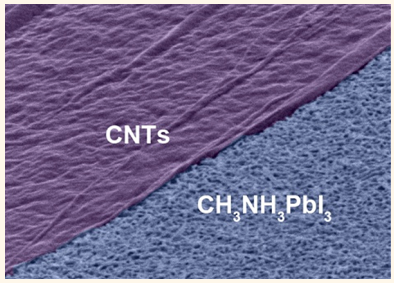

KEYWORDS: perovskite solar cells · carbon nanotubes · laminated · vacuum-free · hole transporter free

In an attempt to reduce the costs of solar cell manufacturing and to increase their potential applications, third-generation photovoltaics are of great interest. These include unconventional light absorber materials with low cost such as dyes,[1] conjugated polymers,[2] and quantum dots,[3] which have triggered continued research efforts. However, these solar cells still lag behind conventional approaches such as Si and GaAs in terms of efficiency. Methylammonium lead halide and mixed halides $CH_3NH_3PbX_3$ (X = Cl, Br, I) possessing the perovskite structure are an emerging light absorber material with features such as large light absorption coefficient, direct band gap,[4] high carrier mobility, and long carrier diffusion length.[5,6] After some early exploration,[7,8] solar cells based on a perovskite absorber have reached an efficiency of more than 15%,[9,10] approaching the efficiency of commercialized c-Si solar cells. The primary advantage of the organic—inorganic halide perovskites is that they can be deposited through a facile solution process, providing avenues for fabricating low-cost solar cells with attractive efficiency.

Evolving from the solid-state dye-sensitized solar cell structure, new device architectures adopting perovskite as a light absorber are emerging, such as planar junctions,[10] where the perovskite material can act as both absorber and charge-transporting material in the solar cell. The hole transport properties of $CH_3NH_3PbI_3$ have enabled perovskite/Au solar cells with power conversion efficiencies reaching 8%.[11,12] This points the way toward a simpler fabrication process that does not involve the utilization of hole-transporting layers. A further simplification of the fabrication process would involve the substitution of the metal electrode layers. Although the perovskite absorber layer is deposited by a simple solution process, the metal electrode of the perovskite solar cell is relatively expensive and deposited by high-vacuum thermal evaporation. To reduce the cost of solar cell fabrication, it is necessary to replace the evaporated metal (Au/Ag) electrode with low-cost materials. Carbon

* Address correspondence to lydiawong@ntu.edu.sg, Nripan@ntu.edu.sg.

Received for review February 24, 2014 and accepted June 12, 2014.

Published online June 13, 2014
10.1021/nn501096h

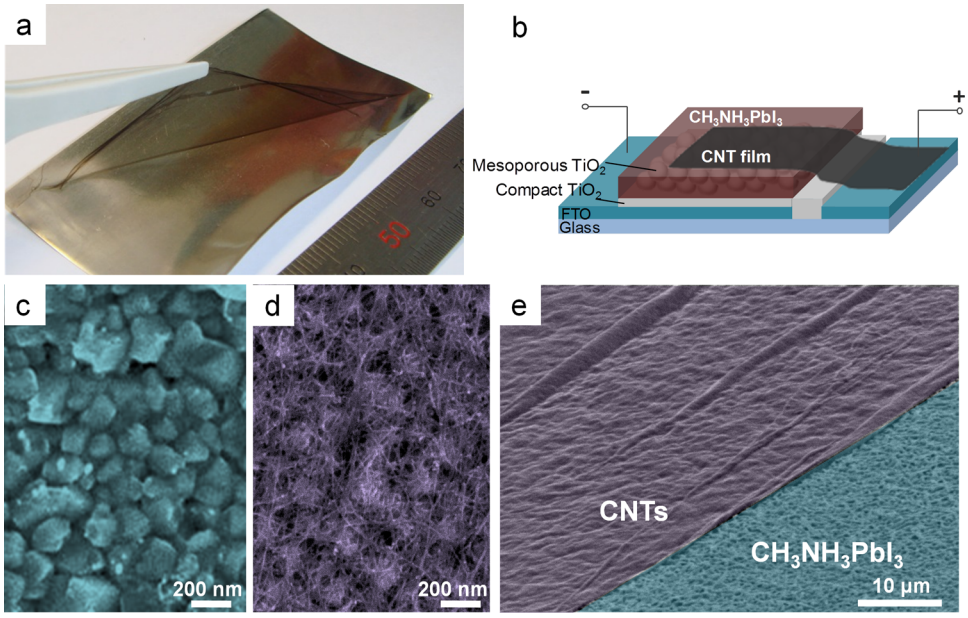

Figure 1. (a) Photo of freestanding CNT film lifting by tweezers to transfer onto other substrates. (b) Schematic of $CH_3NH_3PbI_3$ perovskite solar cell with CNT film electrode. (c) Top view SEM images of $CH_3NH_3PbI_3$ perovskite substrate before and (d) after CNT transfer. (e) Tilted SEM image of $CH_3NH_3PbI_3$ perovskite substrate (blue) partly covered by CNT film (purple).

nanotubes (CNTs), with their excellent electrical conductivity, chemical stability, and unique nanostructure, have been applied as electrodes in CdTe,[13,14] dye-sensitized solar cells,[15,16] and organic solar cells.[17,18] Not only did the CNT electrode show comparable performance to conventional architectures, it also provided the solar cell with more features such as flexibility[15] and semitransparency for tandem solar cells.[19] The recent development of silicon/CNTs solar cells[20] revealed the advantages of CNTs over metallic grids, due to the better local charge collection of the nanometer-scale networks[21] and tunable electrical properties with chemical doping.[22,23]

Here we introduce a facile perovskite solar cell fabrication technique by directly transferring CNT films, exempting the energy-consuming metal deposition process. The $CH_3NH_3PbI_3$/CNTs solar cell showed an efficiency of up to 6.87%, demonstrating the potential of applying carbon nanotubes as a charge collector, eliminating both the metal electrode and hole transporter in perovskite solar cells. The charge transfer and transport in $CH_3NH_3PbI_3$/CNTs solar cells were studied through photoluminescence (PL) and impedance measurements. The addition of the hole transporter 2,2′,7,7′-tetrakis(*N*,*N*-*p*-dimethoxyphenylamino)-9,9′-spirobifluorene (spiro-OMeTAD) improved the efficiency to 9.90%.

RESULTS AND DISCUSSION

The CNT network films were synthesized using a floating catalyst chemical vapor deposition (CVD) method. Details of CNT synthesis and the growth mechanism are described in our previous report.[24] The CNTs in the film were mainly single and double walled, with diameters in the 1−2 nm range (Supporting Information Figure S1), and were of semiconducting and metallic character. The nanotubes were assembled in bundles with diameters of 5−10 nm, which interweaved to form networks. The as-grown CNTs contained a trace amount of Fe catalyst and amorphous carbon on the surface. The Raman spectrum of the as-synthesized CNT film in Figure S2, shows a relatively low defect derived D band intensity as a proof of high purity. Facile transferring is another advantageous feature of the CNT films. According to the floating catalyst growth mechanism, CNTs grew from the floating catalyst particles in the carrier gas flow and formed an aerosol after growth. The aerosol was collected by substrates at the end of the CVD chamber. Once deposited from the aerosol, the CNTs showed strong tube-to-tube interaction and assembled into a freestanding thin film. As shown in Figure 1a, the as-synthesized CNT film was mechanically strong and freestanding. The CNT films are easily peeled off from the substrate by tweezers and transferred to other substrates for device fabrication. Unlike the CNT films attained by filtration or spray or dip coating methods, the as-synthesized freestanding ones do not contain dispersing surfactant, which may hinder charge transport.

The schematic of CNT-based perovskite solar cell structure is shown in Figure 1b. The cell consisted of layers of fluorine-doped tin oxide (FTO)/TiO_2 compact layer/mesoporous TiO_2/$CH_3NH_3PbI_3$/CNT film. In brief, a layer of compact TiO_2 was deposited by spray pyrolysis on FTO glass followed by a layer of mesoporous TiO_2. Subsequently, $CH_3NH_3PbI_3$ was deposited using a sequential deposition method.[9] The freestanding CNT film was placed on top of the perovskite layer, and drops of toluene were added to improve the

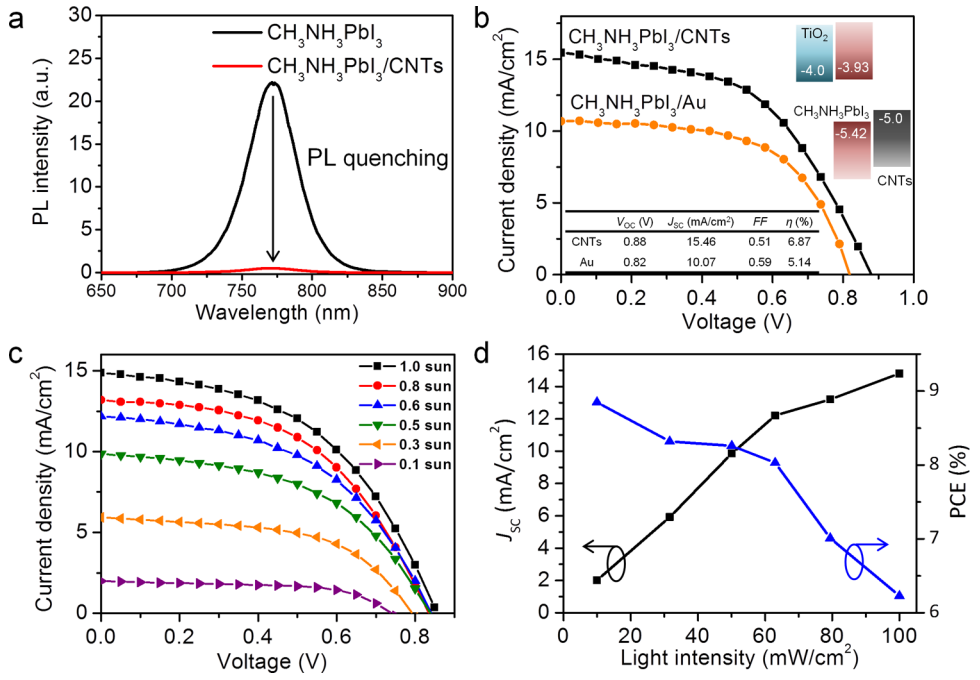

Figure 2. (a) Photoluminescence quenching of $CH_3NH_3PbI_3$ perovskite with CNTs. (b) Characteristic $J-V$ curves of $CH_3NH_3PbI_3$/CNTs and $CH_3NH_3PbI_3$/Au solar cells under AM 1.5, 1 sun condition. Inset: Band diagram of $CH_3NH_3PbI_3$/CNTs perovskite solar cell. (c) Characteristic $J-V$ curves of a $CH_3NH_3PbI_3$/CNTs perovskite solar cell under different illumination. (d) Correlation between J_{SC}, PCE of the $CH_3NH_3PbI_3$/CNTs solar cell, and the incident light intensity.

adhesion. The toluene does not significantly dissolve the $CH_3NH_3PbI_3$ and wets the CNT film, drawing it toward the perovskite substrate by surface tension during vaporization. As a result, the CNT film was well adhered to the perovskite surface by van der Waals force. The electron microscopy images of $CH_3NH_3PbI_3$ perovskite before and after CNT transfer are presented in Figure 1c and d, respectively. Figure 1c shows the formation of a dense layer of $CH_3NH_3PbI_3$ perovskite nanocrystals on top of the mesoporous TiO_2. After transfer, the flexible CNT network could conformally coat the rough surface of perovskite (Figure 1d), enabling an increased interface area between perovskite and CNT as well as an improved electrical contact. Figure 1e showed a false-color tilted SEM image of the perovskite substrate (blue) partly coated with a CNT film (purple). Some folds and wrinkles shown on the CNT film were due to the manual transfer. The single-step direct transfer carried out in ambient atmosphere avoids the requirement of high temperature and high vacuum for metal electrode evaporation.

Photoluminescence quenching is used to demonstrate the charge extraction ability of hole-conducting material in contact with the perovskite.[25] $CH_3NH_3PbI_3$ was deposited on bare quartz and CNT film-covered quartz substrates. The excitation and luminescence measurement was taken from the quartz side for both samples. As shown in Figure 2a the PL of $CH_3NH_3PbI_3$ on bare quartz shows strong luminescence at ~770 nm, which is suppressed in the CNT sample with a quenching ratio of 44 times as a sign of the effective charge transfer from $CH_3NH_3PbI_3$ to CNTs. Carbon nanotubes are a p-type conducting material at ambient atmosphere with a reported work function between −4.95 and −5.05 eV at room-temperature condition.[26] According to the band edge positions of TiO_2, $CH_3NH_3PbI_3$, and CNTs, the band diagram of the perovskite/CNTs solar cell is shown as an inset in Figure 2b. The CNT films provide a significant driving force for the hole injection from the perovskite layer, collecting and transporting holes to the external circuit. A power conversion efficiency (PCE) of 6.87% with a V_{OC} of 0.88 V, J_{SC} of 15.46 mA/cm^2, and fill factor of 0.51 under AM1.5 100 mW/cm^2 illumination was achieved by the best device of $CH_3NH_3PbI_3$/CNTs solar cells (Table S1). The $CH_3NH_3PbI_3$/Au solar cell was also fabricated by directly depositing a Au electrode on top of the perovskite for comparison. $CH_3NH_3PbI_3$/CNTs solar cells present higher V_{OC} and J_{SC} than the Au counterpart; however their fill factor is lower (Figure 2a). Higher V_{OC} and J_{SC} might be due to better hole selectivity of CNTs than metallic Au, reducing the chance of interface recombination. The higher sheet resistance of CNT film (2−5 kΩ as measured by four-point probe) could explain the poorer fill factor. Therefore, removing impurities on the CNT surface to reduce the sheet resistance of the CNT film may improve the cell efficiency in the future.

Photovoltaic performance of the $CH_3NH_3PbI_3$/CNTs solar cell was also tested under different illumination conditions as shown in Figure 2c. The V_{OC} of the solar cell decreased with the decrease of incident light intensity; however, the FF improved at lower light illumination. The correlation between J_{SC} and light

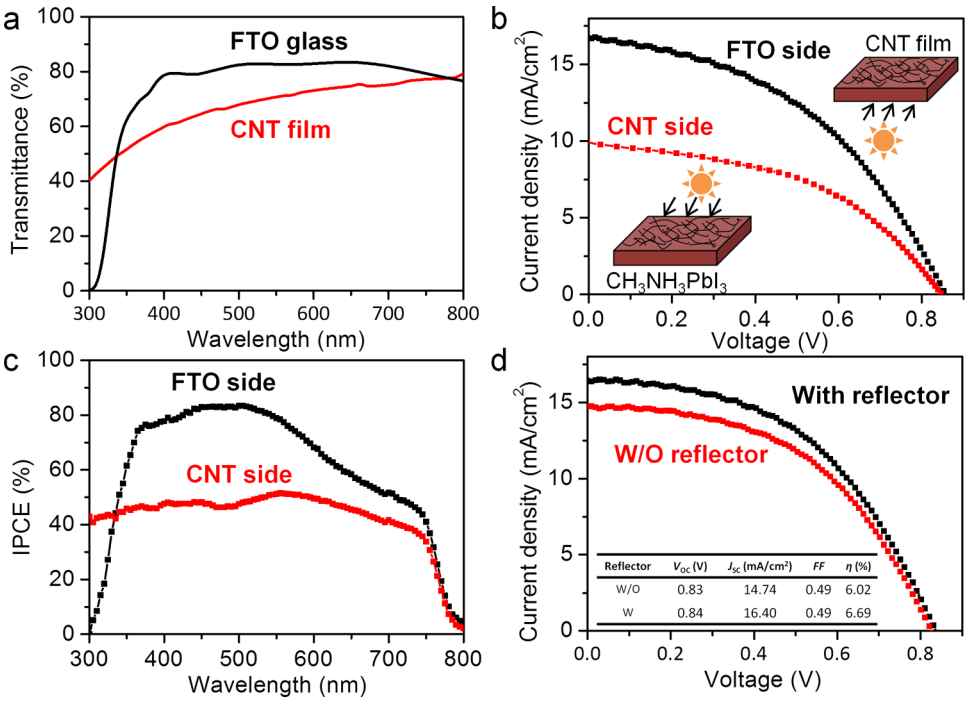

Figure 3. (a) UV−vis transmittance of a CNT film and FTO glass. (b) Light *J*−*V* curves of $CH_3NH_3PbI_3$ perovskite/CNTs solar cell with illumination from the FTO and from the CNT side, under conditions of AM1.5 100 mW/cm^2. (c) IPCE of a $CH_3NH_3PbI_3$ perovskite/CNTs solar cell with illumination from the FTO and from the CNT side. (d) Light *J*−*V* curves of a $CH_3NH_3PbI_3$ perovskite/CNTs solar cell with and without an Al reflector.

intensity is plotted in Figure 2d. The J_{SC} of the solar cell shows a quasi-linear relationship below 0.6 sun. However, at higher light intensity the J_{SC} was lower than the linear extrapolation from low illumination, showing limited charge collection efficiency. Lower FF and suppressed J_{SC} can be justified by the high sheet resistance of the CNT film, increasing the overall series resistance (R_s) of the solar cell. Under these circumstances, the efficiency shows an increasing trend under low light illumination, reaching 8.85% at 10 mW/cm^2. This is especially appealing for indoor applications. Even without the conventional hole-transporting material spiro-OMeTAD, this preliminary result positions CNTs as a promising charge collector for perovskite solar cells. Additionally, since the carbon nanotube film was only a thin membrane with tens of nanometers thickness, there is a great potential for flexible perovskite devices.

The low thickness of CNT network films allows for the perovskite solar cells to be illuminated from both directions. The UV−vis transmittance spectra of a CNT film and bare FTO are compared in Figure 3a. The CNT film (20−50 nm) shows a slightly lower transmittance than the FTO in the visible range. Therefore, unlike the conventional Au electrode, the semitransparent CNT counter electrode can also transmit light, which can be harvested in the solar cell. The *J*−*V* curves of a $CH_3NH_3PbI_3$/CNTs solar cell with FTO and CNT side illumination are shown in Figure 3b. When illuminated from FTO side, the solar cell generates a V_{OC} of 0.86 V, a J_{SC} of 16.7 mA/cm^2, an FF of 0.44, and a PCE of 6.29%. With illumination from the CNT side, the solar cell showed a similar V_{OC} of 0.85 V, a lower J_{SC} of 9.9 mA/cm^2, an FF of 0.46, and a PCE of 3.88%. The double-sided light response feature of the perovskite/CNTs solar cell is an advantage in applications in building integrated photovoltaic applications such as solar cell windows.

Incident photon to electron conversion efficiency (IPCE) of the $CH_3NH_3PbI_3$/CNTs solar cells with illumination from different sides is compared in Figure 3c. With FTO side illumination, the solar cell response wavelength ranged from 300 to 800 nm. The ~800 nm cut-off wavelength corresponds to the 1.55 eV band gap of $CH_3NH_3PbI_3$ perovskite absorber. At shorter wavelengths, the photocurrent is cut off by FTO and TiO_2, as shown in the UV−vis transmittance of FTO. The device shows high photon conversion efficiency, above 70%, for wavelengths from 400 to 600 nm. However, the IPCE is relatively lower at longer wavelength regions possibly due to incomplete absorption of light. UV−vis transmittance spectra of a whole perovskite/CNTs solar cell (Figure S4) show light transmittance starting from 510 nm, which explains the IPCE drop above 510 nm. The lower J_{SC} of the solar cell with light illumination from the CNT side of the solar cell could also be explained by the IPCE results. With illumination from the CNT side, the photoresponse at wavelengths above 350 nm is lower than with the illumination from the FTO side, which is expected

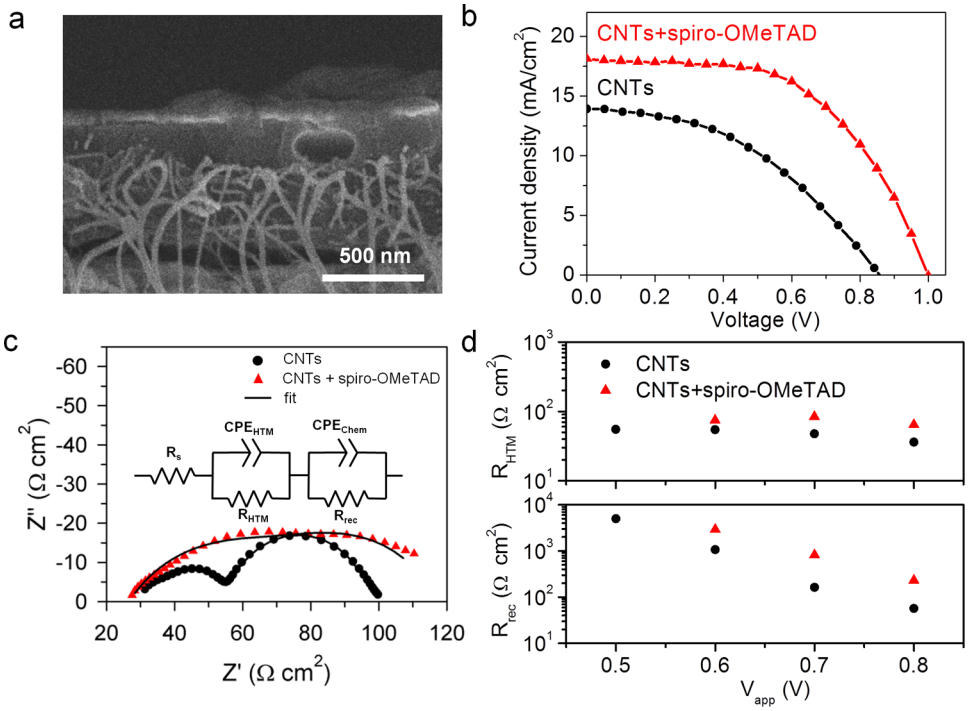

Figure 4. (a) Cross section SEM image of CNT film after spiro-OMeTAD infiltration. (b) *J*−*V* curves of a solar cell with and without spiro-OMeTAD at 1 sun. (c) Nyquist plot of solar cells with and without spiro-OMeTAD measured at 800 mV applied bias under 0.1 sun; fittings represented by solid lines follow the equivalent circuit shown in the inset. (d) Hole-transporting material resistance (R_{HTM}) and recombination resistance (R_{rec}) extracted from fitting of the impedance spectra at different voltages under 0.1 sun illumination.

given the lower transmittance of CNTs with respect to FTO for the 350−800 nm region (Figure 3a). The lower IPCE for CNT side illumination may be related to the poorer charge collection efficiency of CNT film than the mesoporous TiO_2 scaffold. It is conceivable that in a conventional perovskite solar cell the Au back electrode can act as a rear reflector to direct unabsorbed light back into the solar cell and provide higher photocurrent because the perovskite layer in the solar cell is not thick enough for full light absorption in wavelength regions from 300 to 800 nm. Therefore, when an aluminum back reflector is introduced at the CNT side of the $CH_3NH_3PbI_3$/CNTs solar cell, the J_{SC} of the solar cell increases from 14.74 mA/cm^2 to 16.40 mA/cm^2 (Figure 3d).

The porous structure of the CNT film offered the possibility of incorporating hole-transporting materials into the CNT network to improve the heterojunction property of solar cells. Here, we have incorporated conventional hole-transporting material (HTM) spiro-OMeTAD into the $CH_3NH_3PbI_3$/CNTs perovskite solar cell by simple spin coating. From the cross session SEM image in Figure 4a, it is clear that the HTM not only covered the CNT network but also wrapped around the CNT bundles. The HTM penetrates through the pores of the CNT networks and forms direct contact to the perovskite layer. The light *J*−*V* curves of a particular solar cell before and after spiro-OMeTAD coating are shown in Figure 4b. The photovoltaic performance improves significantly with the introduction of spiro-OMeTAD, with V_{OC} increasing from 0.86 V to 1.00 V, J_{SC} from 13.9 mA/cm^2 to 18.1 mA/cm^2, and FF from 0.43 to 0.55. Hence, the efficiency is nearly doubled, from 5.14% to 9.90% (Table S2). The CNT/spiro-OMeTAD composite film provided better coverage over the perovskite surface compared to the porous CNT networks; therefore it maximized the contact interface with the perovskite, which could have a positive effect on both charge separation and collection, resulting in an improvement of J_{SC}. The spiro-OMeTAD infiltrates beneath the CNT network and forms a direct contact with $CH_3NH_3PbI_3$. The higher Fermi level of the hole-transporting material could contribute to the higher V_{OC} for the spiro-OMeTAD devices. The CNT/spiro-OMeTAD solar cells were also tested under rear illumination and showed a lower efficiency of 5.6% (Figure S8) and suffer from light absorption losses in the spiro-OMeTAD layer.

Impedance spectroscopy has been deployed to further understand the electrical characteristics in CNT and CNT/spiro-OMeTAD solar cells. The obtained spectra for both samples clearly show different shapes in all the measured voltages. The measurements in the CNT device result in two arcs separated in frequencies; in contrast, the CNT/spiro-OMeTAD presents a more merged spectrum (Figure 4c). This is probably due to an extra element in the hole transport process: the injection of the holes from the spiro-OMeTAD to the

CNTs, which is supported by the favorable energetics shown in the inset of Figure S6. The higher frequency features of the impedance spectra in this kind of device are commonly attributed to the hole transport, whereas the rest of the spectra contain information about the charge recombination.[27−29] The results were fitted following a previously reported equivalent circuit,[29] where the first distorted arc at higher frequencies accounts for the global hole transport processes including the additional charge transfer process from the spiro-OMeTAD to the CNTs (since the characteristic times for both process are so close that their effective separation is not possible). Since no evident electron transport features are observed, the lower frequency part of the spectra is simplified to an *R-C* circuit whose origin is recombination. The values of the hole transport resistance (R_{HTM}) represented in Figure 4d show slightly higher values when spiro-OMeTAD is added to the CNTs. This increase is the result of the extra charge transfer process needed (from spiro-OMeTAD to CNTs) in this case as well as the lower conductivity of spiro-OMeTAD. The series resistance does not change significantly with the addition of spiro-OMeTAD, as shown in Figure S7, where the total series resistance ($R_s + R_{HTM}$) follows the same trend as R_{HTM}. Dark current curves of the solar cell before and after adding spiro-OMeTAD (Figure S7) showed similar slope at high potential, also indicating similar series resistance for both cells. In contrast, the recombination resistance (R_{rec}) is substantially lower for the CNT device in Figure 4d, indicating a higher carrier recombination for CNT-only devices. This is expected as a consequence of the lower charge selectivity of the CNTs[30] due to the existence of both semiconducting and metallic CNTs within the grown films. Although there is a slight increase in the total hole transport resistance when spiro-OMeTAD is integrated, the reduced recombination (as evidenced by higher recombination resistance) is the more dominant effect. This reduction in recombination is reflected as higher FF and V_{OC} for CNT/spiro-OMeTAD solar cells. This clearly indicates that future studies should focus on tuning the CNT energetics with the intention of improving the selectivity and sheet resistance, which will lead to higher FF and V_{OC} in the CNT devices without the application of an additional HTM.

CONCLUSIONS

To conclude, we have demonstrated the application of direct synthesized CNT network films as a hole collector for perovskite solar cells. The $CH_3NH_3PbI_3$/CNTs perovskite solar cell without hole-transporting material and Au electrode provided a power conversion efficiency of 6.29% under AM 1.5, 100 mW/cm^2 conditions and 8.85% under 10 mW/cm^2 conditions. The efficiency might be improved by future purification and chemical doping of CNTs to increase the film conductivity and increase the work function. Also, the utilization of pure semiconducting CNTs could increase the charge selectivity, improving the solar cell performance. By incorporating the hole-transporting material spiro-OMeTAD, the $CH_3NH_3PbI_3$/CNTs perovskite solar cell efficiency can be further improved to 9.90%. With the advantages of low cost, a facile fabrication process without a vacuum environment, chemical stability, and electrical compatibility to organometal halide perovskite, the CNT electrode is a promising electrode for replacement of expensive Au electrodes in perovskite solar cells. Furthermore, the flexible and transparent CNT film electrodes show great potential in flexible or tandem perovskite solar cells.

EXPERIMENTAL SECTION

Synthesis of CNT Film. CNT network films were synthesized using the floating catalyst chemical vapor deposition method using a tube furnace. Ferrocene (0.36 M) as catalyst and sulfur (0.036 M) as growth promotion agent were dissolved in xylene to form a uniform precursor solution. The temperature for CVD was set to 1150 °C. Then 2500 sccm Ar and 600 sccm H_2 were introduced into the quartz tube as carrier gas. When the temperature and gas flow stabilized, the precursor solution was injected into the quartz tube at a preheating zone of the furnace with a temperature of 180 °C. The precursor vaporized and was transported into the center zone of the furnace by the gas flow for CNT growth. CNTs grew from the floating Fe catalyst in the carrier gas flow. After growth, the CNTs formed an aerosol carried by the gas flow. The CNT aerosol was carried to the end of the quartz tube with a temperature of 100−150 °C, where it was collected on a nickel foil and assembled into a freestanding thin film. More information on CNT film synthesis can be found in a previous report.[24]

Preparation of TiO_2 Substrates. Fluorine-doped tin oxide substrates were laser etched to form the desired pattern. The etched substrates were subsequently cleaned with Decon soap solution, then deionized water, followed by ethanol. A thin layer of compact TiO_2 (80−100 nm, blocking layer) was deposited by aerosol spray-pyrolysis at 450 °C using compressed air as a carrier gas. These substrates were immersed in a 40 mM $TiCl_4$ solution for 30 min at 70 °C, followed by rinsing with deionized water and ethanol. A mesoporous TiO_2 layer (~400 nm) composed of 20 nm-sized particles was then deposited by spin coating and subsequently annealed at 500 °C for 30 min.

Preparation of $CH_3NH_3PbI_3$ Absorber. The organic−inorganic perovskite $CH_3NH_3PbI_3$ was deposited by a sequential method as reported in the literature.[9] PbI_2 (1 M) was dissolved in *N*,*N*-dimethylformamide overnight under stirring conditions at 70 °C. The solution was spin coated on the TiO_2 substrates at 6000 rpm for 5 s, followed by annealing at 70 °C for 30 min. Subsequently the films were dipped in a 8 mg/mL solution of CH_3NH_3I in 2-propanol (IPA) for 20 min. The films were then rinsed further with IPA and dried at 70 °C for 30 min.

Deposition of CNT Film. The edges of the perovskite region were covered by tape. The taped substrates were put under the lifted CNT film and covered by the film. Several drops of toluene were added to wet the CNT film and perovskite surface. After toluene vaporization, CNTs on the unwanted region were removed by wiping with a cotton stick. Both the CNT and FTO were soldered for better electrical contact.

Deposition of spiro-OMeTAD: Hole Transporting Material. Spiro-OMeTAD was dissolved in chlorobenzene (120 mg mL^{-1}) and spin-coated on substrates with a speed of 4000 rpm. Additives such as $Li(CF_3SO_2)_2N$ (29 μL ml^{-1} from a stock solution of 520 mg mL^{-1}), *tert*-butylpyridine (29 μL), and FK102 dopant

(24 μL, stock solution 300 mg mL^{-1}) were added to the above solution.

Solar Cell Characterization. Photocurrent–voltage measurements were carried out using a San-El Electric XEC-301S under AM 1.5 G, and the illumination area was defined by a 4 × 4 mm mask. Incident photon to current conversion efficiency was measured using a PVE300 (Bentham), with a dual xenon/quartz halogen light source, measured in dc mode with no bias light used. Incident light intensity was calibrated using a photodiode detector (silicon calibrated detector, Newport).

Impedance Measurement. IS measurements were carried out under low light intensity (0.1 sun) with an Autolab 302 N. The applied dc bias potential ranged from 100 to 1000 mV. A voltage perturbation with 20 mV (rms) amplitude was applied with a frequency swipe from 1 MHz to 1 Hz. The spectra were fitted using Z-View software.

Material Characterization. HRTEM images of CNTs were recorded using a transmission electron microscope (JEM-2010). Top view and cross sectional images of solar cells were recorded using a field emission scanning electron microscope (JSM-7600F). UV–vis absorption spectra were collected with a Shimadzu UV3600 spectrophotometer. Raman and photoluminescence measurements were taken using a spectrometer (Horiba JY-T64000) under an excitation laser with a wavelength of 532 nm.

Conflict of Interest: The authors declare no competing financial interest.

Acknowledgment. Funding from National Research Foundation (NRF), Singapore, is acknowledged through CRP Award No. NRF-CRP4-2008-03 and the Singapore-Berkeley Research Initiative for Sustainable Energy (SinBeRISE) CREATE program.

Supporting Information Available: HRTEM and Raman spectrum of the CNT film, SEM images and UV–vis spectrum of $CH_3NH_3PbI_3$/CNTs and $CH_3NH_3PbI_3$/spiro-OMETAD/CNTs solar cells, capacitance Bode plots, and series resistance estimates of solar cells are included. This material is available free of charge *via* the Internet at http://pubs.acs.org.

REFERENCES AND NOTES

1. Gratzel, M. Dye-Sensitized Solar Cells. *J. Photochem. Photobiol. C: Photochem. Rev.* **2003**, *4*, 145–153.
2. Gunes, S.; Neugebauer, H.; Sariciftci, N. S. Conjugated Polymer-Based Organic Solar Cells. *Chem. Rev.* **2007**, *107*, 1324–1338.
3. Kramer, I. J.; Sargent, E. H. Colloidal Quantum Dot Photovoltaics: A Path Forward. *ACS Nano* **2011**, *5*, 8506–8514.
4. Kim, H. S.; Lee, C. R.; Im, J. H.; Lee, K. B.; Moehl, T.; Marchioro, A.; Moon, S. J.; Humphry-Baker, R.; Yum, J. H.; Moser, J. E.; *et al*. Lead Iodide Perovskite Sensitized All-Solid-State Submicron Thin Film Mesoscopic Solar Cell with Efficiency Exceeding 9%. *Sci. Rep.* **2012**, *2*, 591.
5. Stranks, S. D.; Eperon, G. E.; Grancini, G.; Menelaou, C.; Alcocer, M. J. P.; Leijtens, T.; Herz, L. M.; Petrozza, A.; Snaith, H. J. Electron-Hole Diffusion Lengths Exceeding 1 Micrometer in An Organometal Trihalide Perovskite Absorber. *Science* **2013**, *342*, 341–344.
6. Xing, G. C.; Mathews, N.; Sun, S. Y.; Lim, S. S.; Lam, Y. M.; Gratzel, M.; Mhaisalkar, S.; Sum, T. C. Long-Range Balanced Electron- and Hole-Transport Lengths in Organic-Inorganic $CH_3NH_3PbI_3$. *Science* **2013**, *342*, 344–347.
7. Kojima, A.; Teshima, K.; Shirai, Y.; Miyasaka, T. Organometal Halide Perovskites as Visible-Light Sensitizers for Photovoltaic Cells. *J. Am. Chem. Soc.* **2009**, *131*, 6050–6051.
8. Im, J. H.; Lee, C. R.; Lee, J. W.; Park, S. W.; Park, N. G. 6.5% Efficient Perovskite Quantum-Dot-Sensitized Solar Cell. *Nanoscale* **2011**, *3*, 4088–4093.
9. Burschka, J.; Pellet, N.; Moon, S. J.; Humphry-Baker, R.; Gao, P.; Nazeeruddin, M. K.; Gratzel, M. Sequential Deposition as a Route to High-Performance Perovskite-Sensitized Solar Cells. *Nature* **2013**, *499*, 316–319.
10. Liu, M. Z.; Johnston, M. B.; Snaith, H. J. Efficient Planar Heterojunction Perovskite Solar Cells by Vapour Deposition. *Nature* **2013**, *501*, 395–398.
11. Etgar, L.; Gao, P.; Xue, Z. S.; Peng, Q.; Chandiran, A. K.; Liu, B.; Nazeeruddin, M. K.; Gratzel, M. Mesoscopic $CH_3NH_3PbI_3$/TiO_2 Heterojunction Solar Cells. *J. Am. Chem. Soc.* **2012**, *134*, 17396–17399.
12. Abu Laban, W.; Etgar, L. Depleted Hole Conductor-Free Lead Halide Iodide Heterojunction Solar Cells. *Energy Environ. Sci.* **2013**, *6*, 3249–3253.
13. Barnes, T. M.; Wu, X.; Zhou, J.; Duda, A.; van de Lagemaat, J.; Coutts, T. J.; Weeks, C. L.; Britz, D. A.; Glatkowski, P. Single-Wall Carbon Nanotube Networks as a Transparent Back Contact in CdTe Solar Cells. *Appl. Phys. Lett.* **2007**, *90*, 243503.
14. Phillips, A. B.; Khanal, R. R.; Song, Z. N.; Zartman, R. M.; DeWitt, J. L.; Stone, J. M.; Roland, P. J.; Plotnikov, V. V.; Carter, C. W.; Stayancho, J. M.; *et al*. Wiring-up Carbon Single Wall Nanotubes to Polycrystalline Inorganic Semiconductor Thin Films: Low-Barrier, Copper-Free Back Contact to CdTe Solar Cells. *Nano Lett.* **2013**, *13*, 5224–5232.
15. Chen, T.; Qiu, L. B.; Cai, Z. B.; Gong, F.; Yang, Z. B.; Wang, Z. S.; Peng, H. S. Intertwined Aligned Carbon Nanotube Fiber Based Dye-Sensitized Solar Cells. *Nano Lett.* **2012**, *12*, 2568–2572.
16. Zhang, S.; Ji, C. Y.; Bian, Z. Q.; Yu, P. R.; Zhang, L. H.; Liu, D. Y.; Shi, E. Z.; Shang, Y. Y.; Peng, H. T.; Cheng, Q.; *et al*. Porous, Platinum Nanoparticle-Adsorbed Carbon Nanotube Yarns for Efficient Fiber Solar Cells. *ACS Nano* **2012**, *6*, 7191–7198.
17. Chaudhary, S.; Lu, H. W.; Muller, A. M.; Bardeen, C. J.; Ozkan, M. Hierarchical Placement and Associated Optoelectronic Impact of Carbon Nanotubes in Polymer-Fullerene Solar Cells. *Nano Lett.* **2007**, *7*, 1973–1979.
18. Ulbricht, R.; Lee, S. B.; Jiang, X. M.; Inoue, K.; Zhang, M.; Fang, S. L.; Baughman, R. H.; Zakhidov, A. A. Transparent Carbon Nanotube Sheets as 3-D Charge Collectors in Organic Solar Cells. *Sol. Energy Mater. Sol. C* **2007**, *91*, 416–419.
19. Xia, X. Y.; Wang, S. S.; Jia, Y.; Bian, Z. Q.; Wu, D. H.; Zhang, L. H.; Cao, A. Y.; Huang, C. H. Infrared-Transparent Polymer Solar Cells. *J. Mater. Chem.* **2010**, *20*, 8478–8482.
20. Wei, J. Q.; Jia, Y.; Shu, Q. K.; Gu, Z. Y.; Wang, K. L.; Zhuang, D. M.; Zhang, G.; Wang, Z. C.; Luo, J. B.; Cao, A. Y.; *et al*. Double-Walled Carbon Nanotube Solar Cells. *Nano Lett.* **2007**, *7*, 2317–2321.
21. Jia, Y.; Wei, J. Q.; Wang, K. L.; Cao, A. Y.; Shu, Q. K.; Gui, X. C.; Zhu, Y. Q.; Zhuang, D. M.; Zhang, G.; Ma, B. B.; *et al*. Nanotube-Silicon Heterojunction Solar Cells. *Adv. Mater.* **2008**, *20*, 4594–4598.
22. Li, Z. R.; Kunets, V. P.; Saini, V.; Xu, Y.; Dervishi, E.; Salamo, G. J.; Biris, A. R.; Biris, A. S. Light-Harvesting Using High Density p-Type Single Wall Carbon Nanotube/n-type Silicon Heterojunctions. *ACS Nano* **2009**, *3*, 1407–1414.
23. Wadhwa, P.; Liu, B.; McCarthy, M. A.; Wu, Z. C.; Rinzler, A. G. Electronic Junction Control in a Nanotube-Semiconductor Schottky Junction Solar Cell. *Nano Lett.* **2010**, *10*, 5001–5005.
24. Li, Z.; Jia, Y.; Wei, J. Q.; Wang, K. L.; Shu, Q. K.; Gui, X. C.; Zhu, H. W.; Cao, A. Y.; Wu, D. H. Large Area, Highly Transparent Carbon Nanotube Spiderwebs for Energy Harvesting. *J. Mater. Chem.* **2010**, *20*, 7236–7240.
25. Docampo, P.; Ball, J. M.; Darwich, M.; Eperon, G. E.; Snaith, H. J. Efficient Organometal Trihalide Perovskite Planar-Heterojunction Solar Cells on Flexible Polymer Substrates. *Nat. Commun.* **2013**, *4*, 2761.
26. Shiraishi, M.; Ata, M. Work Function of Carbon Nanotubes. *Carbon.* **2001**, *39*, 1913–1917.
27. Dualeh, A.; Moehl, T.; Tetreault, N.; Teuscher, J.; Gao, P.; Nazeeruddin, M. K.; Gratzel, M. Impedance Spectroscopic Analysis of Lead Iodide Perovskite-Sensitized Solid-State Solar Cells. *ACS Nano* **2014**, *8*, 362–373.
28. Kim, H. S.; Lee, J. W.; Yantara, N.; Boix, P. P.; Kulkarni, S. A.; Mhaisalkar, S.; Gratzel, M.; Park, N. G. High Efficiency Solid-State Sensitized Solar Cell-Based on Submicrometer Rutile TiO_2 Nanorod and $CH_3NH_3PbI_3$ Perovskite Sensitizer. *Nano Lett.* **2013**, *13*, 2412–2417.

29. Gonzalez-Pedro, V.; Juarez-Perez, E. J.; Arsyad, W.-S.; Barea, E. M.; Fabregat-Santiago, F.; Mora-Sero, I.; Bisquert, J. General Working Principles of $CH_3NH_3PbX_3$ Perovskite Solar Cells. *Nano Lett.* **2014**, *14*, 888–893.
30. Juarez-Perez, E. J.; Wuβler, M.; Fabregat-Santiago, F.; Lakus-Wollny, K.; Mankel, E.; Mayer, T.; Jaegermann, W.; Mora-Sero, I. Role of the Selective Contacts in the Performance of Lead Halide Perovskite Solar Cells. *J. Phys. Chem. Lett.* **2014**, *5*, 680–685.